

Compressive Sensing Mapping System for Spatial Characterization of Photovoltaic Devices

Samuel Adrian Cerezo

FAIN

Universidad Nacional del Comahue

Neuquén, Argentina

samueladriancerezo@gmail.com

Dr. Matías Andrés Córdoba

FAIN, PROBIEN, CONICET-UNCo

Universidad Nacional del Comahue

Neuquén, Argentina

matiasandrescordoba@gmail.com

Dr. Fernando Pérez Quintián

FAIN, IITCI, CONICET-UNCo

Universidad Nacional del Comahue

Neuquén, Argentina

fernando.perez.quintian@gmail.com

Abstract—Photocurrent mapping (PM) is a non-destructive characterization method of solar cells and panels. It is used in the industry for quality control in the production of photovoltaic devices, in scientific laboratories to characterize new materials, and in photovoltaic facilities to find module failures. The PM consists of applying a laser light beam perpendicularly on a photovoltaic device, scanning the surface point by point, and measuring the induced current as a function of the position of the beam. These systems require a high degree of mechanical stability, which leads to an increase in the characterization times when the area is large. In recent years, it has been made progress in the use of compressive sensing algorithms applied in PM tests in order to reduce moving parts and the measuring times. In this work we apply the compressive sensing technique to obtain a photocurrent map of Si photovoltaic devices. Results are compared with the ones obtained by the conventional technique.

Index Terms—Compressive sensing, photovoltaic, light beam induced current (LBIC) measurement, Walsh-Hadamard basis, DCT basis.

I. INTRODUCTION

Scanning techniques have been used for the characterization and study of semiconductors and solar cells since the late 1970s [1]. The photocurrent mapping (PM) technique is a non-destructive characterization method for photovoltaic devices used both at industrial and laboratory level to characterize preparation methods and novel materials, and in photovoltaic installations to find module failures. This technique allows detecting damage produced in a solar panel that cannot be perceived by the human eye, such as that resulting from a hail fall, where the damaged semiconductor can leave important areas of the panel non-functional [2] [3]. Typical PM systems consist of a mechanical x-y table containing stepper motors that are responsible for moving a laser beam over the sample area, measuring the short-circuit current on a point-to-point basis. Current variations on the surface are caused due to cell defects and impurities. The scanning is performed mechanically and can be of two types: the fixed sample and the moving beam or the fixed beam and the moving sample [4]. This technique, which induces a current by projecting a beam of light onto the cell, is known as LBIC (Light Beam Induced Current). LBIC technique requires a high degree of mean stability due to the need for micrometric spatial resolutions. For this reason, the LBIC method presents long times when a sufficiently

large area needs to be analyzed. Thus, alternative methods that do not involve moving parts during the measurement are welcomed.

In recent years, an alternative methodology to perform the PM has been investigated using a concept called compressive sensing (CS) [5] [6] [7] [8], which does not involve the use of moving parts for the process of acquiring current values. The concept of CS stems from the image compression techniques widely used today, such as JPEG, which uses the DCT (discrete cosine transform) or the Wavelet transform. With this, it is possible to represent an image with a smaller amount of information. Since the CS requires a smaller number of current measurements than the conventional PM and no moving parts are needed for a point-to-point scan, the measurement speed with respect to the conventional method can be significantly increased [9].

Regarding the latest advances in the application of CS to obtain PM, in 2016 Cashmore et al. [10] described the use of CS applied to solar cells, in which they implement random measurement matrices instead of directly projecting an orthogonal basis. To perform the measurements, they use a laser together with a micromirror array. When the results are compared with those obtained by electroluminescence, CS achieves a considerable increase in the measurement speed. In the same year, Koutsourakis [5] demonstrated that a commercial projector can be effectively used for the projection of the patterns on the sample. The results show that with this methodology, neither a good level of precision nor a good level of resolution is achieved, however, the system is low cost compared to conventional methods. In 2017, Quan et al. [8] proposed a fast and efficient system for locating defects in solar cells. Unlike the aforementioned cases, in that work the authors place the cell face to face with an LCD monitor, in which the patterns are displayed on the screen. In 2019, Quan et al. [6] proposed an effective method for cell defect detection by combining compressive sensing and image processing. By using an optical camera to obtain the a priori location of the cell characteristics, the defects in the semiconductor can be found more effectively, since the compressive sensing is only responsible for detecting the defects in the semiconductor. The system uses a laser in conjunction with a micromirror array to project the patterns.

The results show that with 2% of the measurements, the cell defects are located. In [11] Zhang et al. proposed an optical technique that can simultaneously acquire functionality and structure images of a single or multiple photovoltaic devices. The method is able to give reliable results with much fewer measurements than image pixels by exploiting the sparsity of functionality and structure images in the Fourier domain. In the same year, the signal amplification advantages of compressed sensing current mapping are presented [12]. In that work, the authors demonstrated that the sparsity of the patterns used for compressive sampling can be controlled to achieve significant signal amplification of at least two orders of magnitude, while maintaining or increasing the accuracy of measurements. Finally, in 2022 Koutsourakis et al. presented the mathematical background and the experimental approach toward megapixel resolution. Combining micromirror devices with CS theory, ultrafast compressed sensing current mapping is presented, overcoming previous computational and experimental barriers.

The present work consists of the design and implementation of a system to obtain the PM of a photovoltaic device using the CS technique. The first stage of the system consists of projecting different patterns on the photovoltaic device; the photocurrent produced by each of them is stored in the PC. Having all the stored current values, the next stage is the reconstruction of the PM with the acquired current information. For this, a mathematical algorithm is used to solve an optimization problem, where the noise level in the reconstructed image is minimized. In this algorithm, the projected images, the measured current values and certain configuration parameters are entered, and the photocurrent map of the solar cell is returned to the output. Different bases were used in the reconstruction algorithm and the results obtained with different photovoltaic devices are compared with the conventional LBIC technique.

This paper is organized as follows. At first, a theoretical formulation of the problem is given, in which the mathematical concepts involved are reviewed. Starting from this basis, the parts of the proposed CS system are described. Then, the results obtained are presented and finally, the main ideas to be highlighted are concluded.

II. PROBLEM FORMULATION

The current map for a photovoltaic device corresponds to a image $h \in \mathbb{R}^{P \times Q}$ that when rearranged is a vector $x \in \mathbb{R}^N$, where $N = P * Q$. In turn, x can be expressed in terms of an orthonormal basis $\Psi = \{\psi_i\}_{i=1}^N$, so the map is represented by (1).

$$x = \sum_{i=1}^N \psi_i s_i = \Psi s \quad (1)$$

The signal x is called K-sparse in the Ψ basis if it has at most K nonzero components and the rest components are zeros [13] [14]. If $K \ll N$, the signal can be stored in that basis without loss of information occupying much less memory and the signal is then said to be compressible. If in the base Ψ there were few coefficients of large value and the rest of small value,

only the largest coefficients can be stored and the signal will be compressible although some information will be lost [15]. If one could know in advance in which base the signal to be measured is sparse, it would be sufficient to measure the $K \ll N$ values corresponding to the coefficients of the signal in that base, i.e. it would be sufficient to make K measurements. According to (1) only the projections $s = \Psi^{-1}x$ for the non-zero values of s would have to be measured.

We denote $y \in \mathbb{R}^M$ as the vector containing the measurements of the signal x . Each measurement will be a linear combination of the values of x , so it can be thought of as an inner product between x and a vector ϕ_j ($j = 1, \dots, M$). Rearranging the vectors ϕ_j in the rows ϕ_j^T forms a matrix $\Phi \in \mathbb{R}^{M \times N}$ called measurement matrix. Substituting Ψ from (1), we obtain (2).

$$y = \Phi x = \Phi \Psi s = \Theta s \quad (2)$$

The matrix $\Theta \in \mathbb{R}^{M \times N}$ must satisfy two conditions: the principle of restricted isometry [16] and the incoherence property [17]. The direct construction of the matrix Φ such that $\Theta = \Phi \Psi$ fulfills both conditions is very difficult to achieve, however both can be achieved with high probability by means of a random Φ matrix of Bernoulli type [18] [19]. These conditions are fulfilled with high probability if (3) is accomplished.

$$M \geq cK \log(N/K) \quad (3)$$

In (3) M is the minimum number of measurements needed to recover the signal x , K is the number of non-zero components that the representation of the signal x has in the basis Ψ , N is the dimension of the signal x and c is a positive constant [9] [20]. This constant depends on the dimensions of the measurement matrix Φ . In the particular case analyzed in [21], c is empirically determined.

Once Φ has been defined and the M measurements have been made, the algorithm should be able to obtain the values of the vector s by solving the inverse problem $y = \Theta s$. This is an ill-conditioned problem, i.e., there are many and significantly different solutions, so the algorithm is asked to impose some constraint on s . In [9] [22] the authors show that minimizing the l_1 norm and minimizing the Total Variation (TV) are suitable for solving this inverse problem. After the minimization process, the map corresponding to the photovoltaic device x is obtained by $x = \Psi s$.

A. Minimizing the l_1 norm

A first option naturally is to ask for the minimum number of non-zero elements of the vector s , since it is the sparse representation of x , so the minimization problem is represented by (4).

$$\min_s \quad \|s\|_{l_1} = \sum_i |s_i| \quad st \quad \Theta s = y \quad (4)$$

The advantage of using (4) is that it is simpler to solve using modern techniques belonging to the convex optimization theory [23].

B. Minimizing the Total Variation

Another alternative condition to impose on s when trying to solve the equation (2) is to ask for a minimum TV. The TV of a two-dimensional image $h \in \mathbb{R}^{P \times Q}$ is defined in (5).

$$TV(h) = \sum_{p=1}^P \sum_{q=1}^Q \sqrt{|h_{p+1,q} - h_{p,q}|^2 + |h_{p,q+1} - h_{p,q}|^2} \quad (5)$$

The following section explains how theoretical concepts are applied in the proposed CS system. It begins with a general description of the stages. After that, the three processes involved are developed: configuration, measurement and reconstruction.

III. CS SYSTEM LAYOUT

The elements composing the system are shown in Fig. 1. Although not shown in the image, these elements are connected to the PC. All this assembly is performed on an optics table that minimizes mechanical vibrations. For the validation tests, commercial and laboratory solar cells were used, which were soldered by means of tin and liquid silver in a sample holder.

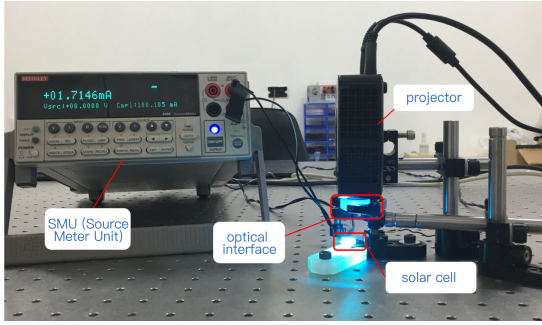


Fig. 1. Arrangement of elements in the CS system mounted

A. Experimental set-up

The scheme of experimental set-up is shown in Fig. 2, where the three stages are displayed in different colors. The user starts a measurement using the graphical interface (GUI) stored in the computer (PC). The projector is used for imaging the patterns on the cell. A lens is used to modify the size of projected patterns. Finally, the current values are obtained by a SMU (Source Meter Unit) Keithley 2400 and stored in the PC. After this process, an optimization algorithm returns the photocurrent map through a minimization function.

B. Measurement process

The measurement process consists of obtaining M measurements of a signal x , which in this case represents the photocurrent map of the cell. Each measurement is obtained by performing the product between the signal x and a matrix ϕ_j ($j = 1, \dots, M$). Each one of these M matrices has 64 rows by 64 columns and is randomly generated with values 1 and 0. In turn, this matrix is equivalent to an image called *pattern* that consists of small squares called *pixels*. A black

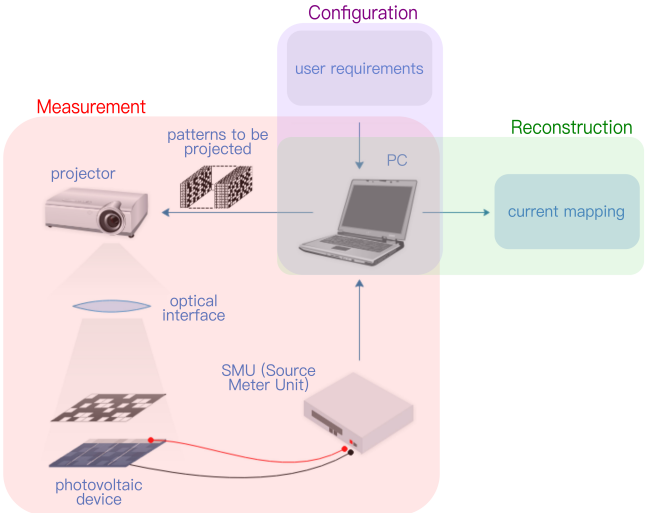


Fig. 2. General CS system diagram. The three stages are in different colors

pixel corresponds to the value 0, and similarly a white pixel corresponds to 1.

The randomly generated pattern is projected onto the solar cell as shown in the Fig. 3.

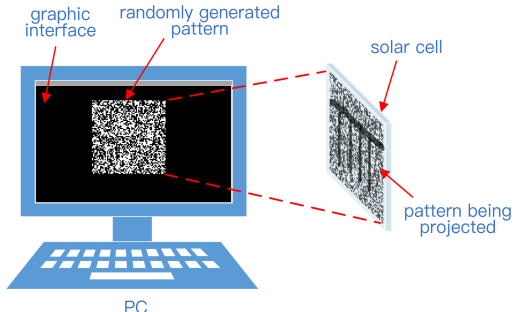


Fig. 3. Schematic showing a 64x64 pattern being projected onto a solar cell

Fig. 4 shows the measurement process represented in mathematical form, in order to visualize the relationship between the measurement process and the mathematical problem to be solved. In this figure the process is carried out as an example taking $M = 4$ measurements by means of four 3×3 patterns. In the following section the results are shown in real samples using 64x64 patterns.

The purple square in Fig. 4 represents the actual PM of cell x which is rearranged as a column vector. The projected patterns, or equivalently the ϕ_j matrices, are rearranged as rows to form the measurement matrix Φ . By projecting the M patterns onto the cell and acquiring the M photocurrent values, what is being done mathematically is a multiplication between the measurement matrix Φ and the actual PM of the cell x , to obtain the measurement vector y . Therefore, the aforementioned inverse problem $\Phi x = y$ is expressed. The latter is solved in the reconstruction process, to find the photocurrent map of the cell.

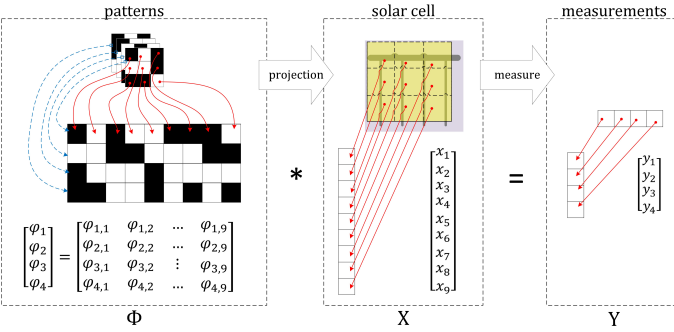


Fig. 4. Example of a measurement process using 3x3 pixel patterns. The vector x represents the photocurrent map of the cell. The current measurements are stored in a y vector.

C. Reconstruction process

The mathematics involved in compressive sensing ensures that a good representation of the photocurrent map x is achieved, without knowing in advance the basis on which this representation is sparse. Then, taking s as the sparse representation of x in orthonormal basis $\Psi = \{\psi_i\}_{i=1}^N$, one can express x as follows:

$$x = \sum_i^N \psi_i s_i = \Psi s \quad (6)$$

Therefore, the inverse problem $\Phi x = y$ is reformulated as follows:

$$\Phi x = \Phi \Psi s = \Theta s = y \quad (7)$$

In this new approach of the inverse problem, now the measurement matrix is another one (Θ) and the unknown is also another one (s). This new matrix Θ results from the multiplication between Φ and Ψ , therefore it still fulfills the necessary conditions for the compressive sensing process. Now the inverse problem is expressed according to (7), although it remains to know which is the proper basis Ψ where the PM representation is sparse.

In solar cells, the conventional shape and geometry of the contact grid is similar to horizontally and vertically distributed stripes. If there is any Ψ basis whose elements are images with this kind of shapes, that would be a suitable basis, since the cell geometry could be represented with few elements [24]. A priori it is not known in which basis the PM representation is sparse, however both the DCT (Discrete Cosine Transform) basis and the Walsh-Hadamard basis are presented as possible options, since both have the elementary shapes mentioned.

Whatever the basis on which the PM is reconstructed, the measurement process is performed with the randomly generated Φ matrix. Then, depending on the basis selected by the user (DCT or Hadamard), the resulting θ matrix is generated. Therefore, it is important to note that in this CS technique, the measurement is the same regardless of the basis that is then chosen to try to reconstruct the photocurrent map.

After making the M measurements to form the vector y and determining the basis on which it is reconstructed, it is

possible to reconstruct the photocurrent map s (expressed in a basis Ψ) by solving the problem $y = \Theta s$. Since this is an ill-conditioned inverse problem, there exist many s that satisfy it, so some additional condition is imposed on s . For this CS system, two conditions were tested: minimize the l_1 norm or minimize the TV. The algorithms used to reconstruct the current map own to the $l1_{magic}$ collection, which is a series of freely available MATLAB® routines for solving compressive sensing problems [25]. The vector s obtained by the algorithm is the representation of the PM of the cell in the Ψ basis. What remains is to obtain the representation of the PM in the canonical basis ($x = \Psi s$).

D. Configuration process

Using the graphical interface of the CS system installed on the PC, it is possible to configure the following parameters:

- Resolution: Patterns of different number of pixels can be projected: 16x16, 32x32, 64x64, 128x128, 256x256.
- COM Port: The serial communication port to which the SMU is connected is selected.
- ratio (M/N): This is a measure of the number of patterns to be projected. For example, if a resolution of 64x64 is chosen and $ratio = 10\%$, then 410 patterns will be projected ($10/100 * 64 * 64 = 410$).
- Range: This is the range of photocurrent values expected in each projection. This depends on the cell to be characterized and its photovoltaic conversion capability. You can select: 0-100 mA, 0-10 mA, 0-1 mA, 0-600 μ A.
- Color: The color of the projected patterns can be changed.
- Name: under which the file with the data obtained by the measurement is saved.

IV. EXPERIMENTAL RESULTS

In this section the results of measurements on three Si devices with different dimensions and defect geometry are shown. The LBIC results are compared with the PM results obtained by CS with different reconstruction bases and optimization algorithms.

Si-solar cell 1. The first sample to be measured is a 17x17 mm^2 Si cell of commercial type. Fig. 5A shows a real photo of the solar cell with a 3 mm^2 rectangular defect placed on the surface, in order to observe if the CS system is able to detect it. The PM obtained by the CS system is shown in Fig. 5B. For this measurement, 64x64 pixel patterns are projected, so that each pixel has an area of 310x310 μm^2 . The reconstruction of the PM is performed by minimizing the TV and using the DCT as the mathematical basis. For this reconstruction, 50% of the patterns were used. This value is determined as follows:

$$percentage[\%] = \frac{M}{N} * 100$$

Where:

- M is the number of patterns projected during the measurement process.
- N is the number of pixels each pattern has. For example, a 64x64 pattern has $N = 64 * 64 = 4096$ pixels.

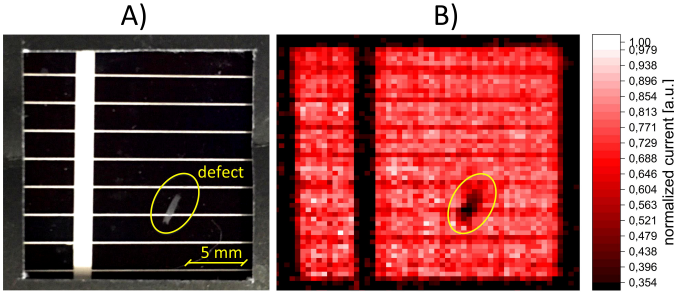


Fig. 5. Measurement of a $17 \times 17 \text{ mm}^2$ silicon sample on which a 3 mm rectangular defect was placed. 64×64 patterns are used. A) Photo of the silicon sample. B) PM obtained by the SC system using the 50% pattern during the measurement.

The next set of measurements is performed on the same Si-solar sample, but now on a region of smaller area, approximately $7 \times 7 \text{ mm}^2$. Two defects were also added: a semicircular one that has a radius of 1 mm , and a smaller one that occupies an area of 1 mm^2 . For this case, the optical stage is modified by changing the lens to one of shorter focal length. By using 64×64 patterns, the area of each pixel is equal to $86 \times 86 \text{ mm}^2$. Fig. 6A shows a photo of the cell and Fig. 6 B-E the photocurrent maps. These results are obtained by minimizing the TV and using the DCT basis. With the 30% of the patterns, it is possible to clearly distinguish the shape and location of the defects. It is also possible to distinguish the contact grid. As an undesired effect, a background grid is visible in this PM. It is intuited that the origin of this effect is given by the DCT base on which it is reconstructed, since the base has in the elements that compose it, vertical and horizontal stripes similar to those observed in the mentioned grid. With 50% and 70% the image does not present relevant improvements. Percentages higher than 70 % generated distortion in the PM obtained.

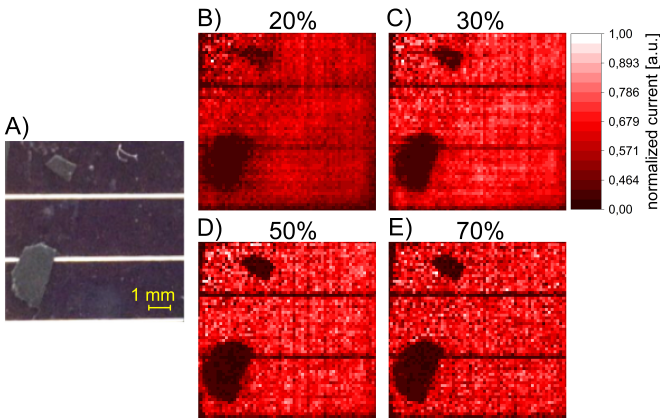


Fig. 6. Measurement of a $7 \times 7 \text{ mm}^2$ silicon sample on which defects of various shapes and sizes were placed. 64×64 patterns are used. For reconstruction, TV is minimized and the DCT basis is used. A) Photo of the sample. B-E) PM obtained by the SC system using different percentages of patterns during the measurement.

Si-solar cell 2. The next sample to be measured is a concentrator Si cell with 3 mm in diameter. Fig. 7A shows a real photo of the sample. The conventional PM (LBIC) is shown in Fig. 7B whereas CS result is in Fig. 7C. Both results have the same resolution, in order to be able to compare the results. In the CS result, the boundary between silicon and metal can be clearly seen. As in the last case, it is possible to distinguish a contact grid.

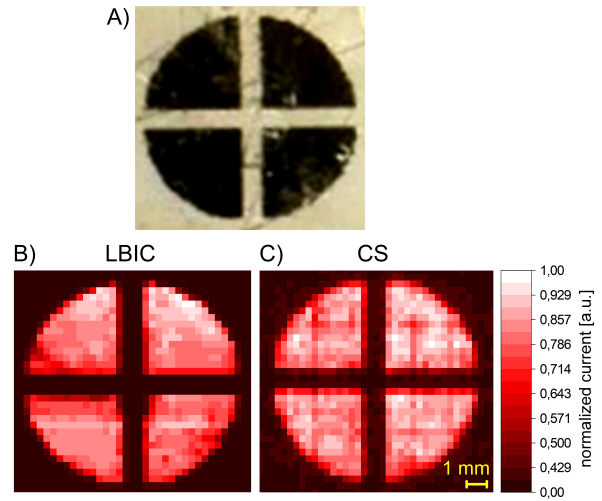


Fig. 7. A characterized silicon cell from a PV concentrator system. A) Photograph. B) 64×64 LBIC current map. C) 64×64 compressive sensing reconstructed current map using 50% (2048) projected patterns

To measure the degree of similarity between both maps, the correlation factor R is used. The correlation factor R between the PM corresponding to the LBIC (L) and the PM obtained by the CS system (x) is defined as:

$$R(L, x) = \frac{\sum_p \sum_q (L_{pq} - \bar{L})(x_{pq} - \bar{x})}{\sqrt{\left(\sum_p \sum_q (L_{pq} - \bar{L})^2\right)\left(\sum_p \sum_q (x_{pq} - \bar{x})^2\right)}} \quad (8)$$

Where \bar{L} is the average intensity of the PM corresponding to the LBIC and \bar{x} is the average intensity of the PM obtained by the CS system. The value of R approaches one as the PM of the CS system resembles that obtained by the LBIC.

Correlation values using Hadamard (Fig. 8A) and DCT (Fig. 8B) basis are shown. In both cases, the results are performed minimizing the l_1 norm and the TV. Different percentages of patterns are used, starting with 1%. When measuring with the 50% of patterns using DCT the value of R is 0.943, while with Hadamard this value is reached with 90%. In Fig. 8A a drop in the curve is observed when using the TV minimization technique. This is due to the fact that the patterns being projected do not form a base per se, therefore, the information obtained in one pattern may be contained in another, causing the algorithm to diverge. In short, measuring with a larger number of patterns does not imply a better estimation of the PM.

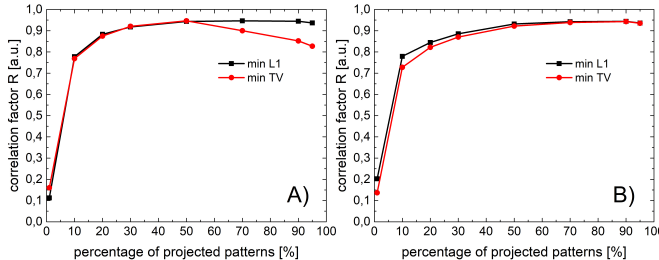


Fig. 8. Correlation factor R between the PM obtained by LBIC and the different PMs obtained by the CS system. Each PM of the CS system has a value of R that depends on the number of patterns that are projected. A) Results when reconstructing using the DCT basis. B) Results when using the Hadamard basis.

V. CONCLUSION

In this work, a system for the characterization of photovoltaic devices without moving parts using CS techniques was designed and implemented. A GUI was programmed, which make it easy for the user to configure different measurement parameters, including the size, color and number of the patterns to be projected and parameters related to the communication between the PC and the SMU. To reconstruct the PM from the measurement, the SC system offers the possibility to use the TV or l_1 minimization algorithm and to do it in the DCT basis or in the Hadamard basis.

Commercial and laboratory solar cells were measured and the results were validated with those obtained by the LBIC method. The results obtained on the samples reveal that when comparing the DCT basis with the Hadamard basis, the former needs a lower percentage of patterns to obtain the best PM.

The main advantage of this CS system is the fact that it does not use moving parts to obtain the PM of a sample. In addition, it is easier to adapt to operate in-situ, whereas with the LBIC method the user would encounter greater complications. In contrast, the disadvantage of the CS system is that it requires a large computational capacity if results with resolutions higher than 64x64 pixels are to be achieved. The development of this PM system using CS techniques was a first step towards a system capable of characterizing photovoltaic devices. Some improvements and refinement strategies emerge from this work. Referring to measure time, the duration of a measurement could be reduced by developing a microcontroller-based current measurement device capable of taking more than one sample per second. Other mathematical bases and minimization algorithms can be explored, as well as other mathematical methods to solve the inverse problem. In addition, the use of an optical camera could be explored to obtain information on the geometry of the sample, while the CS would only have to locate the defects.

ACKNOWLEDGMENT

This work was supported by a grant from Universidad Nacional del Comahue (UNCo): PIN 2018 04/I24.

REFERENCES

- [1] T. Marko, J. Krc, and I. Sorli, *45th International Conference on Microelectronics, Devices and Materials and the Workshop on Advanced Photovoltaic Devices and Technologies*, Ljubljana, 2009.
- [2] M. Arnaud, S. Michael, K. Iris, M. Gerhard, and M. Kontges, “Detecting Photovoltaic Module Failures in the Field During Daytime With Ultra-violet Fluorescence Module Inspection,” *IEEE Journal of Photovoltaics*, vol. 7, no. 6, pp. 1710–1716, 2017.
- [3] M. Wolfgang, E. G. C, V. Yuliya, S. Markus, S. Horst, K. Karl, E. Rita, U. Gusztav, and H. Christina, “Outdoor detection and visualization of hailstorm damages of photovoltaic plants,” *Renewable Energy*, vol. 118, pp. 138–145, 2018.
- [4] C. J., P. G., B. J., and H. Föll, “CELLO: an advanced LBIC measurement technique for solar cell local characterization,” *Solar Energy Materials and Solar Cells*, vol. 76, no. 4, pp. 599–611, 2003.
- [5] K. George, C. Matt, H. S. R. G., B. Martin, B. T. R., and G. Ralph, “Compressed Sensing Current Mapping Spatial Characterization of Photovoltaic Devices,” *IEEE Journal of Photovoltaics*, vol. 7, no. 2, pp. 486–492, 2017.
- [6] Q. Lei, X. Kai, L. Yan, and Z. Hanlu, “Camera enhanced compressive light beam induced current sensing for efficient defect detection in photovoltaic cells,” *Solar Energy*, vol. 183, pp. 212–217, 2019.
- [7] K. George, C. Matt, B. Martin, H. S. R. G., B. T. R., and G. Ralph, “Compressed sensing current mapping methods for PV characterisation,” in *2016 IEEE 43rd Photovoltaic Specialists Conference (PVSC)*. Portland, OR, USA: IEEE, 2016, pp. 1308–1312.
- [8] Q. Lei, X. Kai, X. Ruoyao, and L. Yan, “Compressive light beam induced current sensing for fast defect detection in photovoltaic cells,” *Solar Energy*, vol. 150, pp. 345–352, 2017.
- [9] C. E.J., R. J., and T. Tao, “Robust uncertainty principles: exact signal reconstruction from highly incomplete frequency information,” *IEEE Transactions on Information Theory*, vol. 52, no. 2, pp. 489–509, 2006.
- [10] C. M. T., K. George, and S. R. G. Gottschalg, Ralph y Hall, “Optical technique for photovoltaic spatial current response measurements using compressive sensing and random binary projections,” *Journal of Photonics for Energy*, vol. 6, no. 2, pp. 25–508, 2016.
- [11] Z. Zhang, M. Yao, X. Li, Q. Deng, Q. Peng, and J. Zhong, “Simultaneous functional and structural imaging for photovoltaic devices,” *Solar Energy Materials and Solar Cells*, vol. 193, pp. 101–106, May 2019.
- [12] G. Koutsourakis, J. C. Blakesley, and F. A. Castro, “Signal Amplification Gains of Compressive Sampling for Photocurrent Response Mapping of Optoelectronic Devices,” *Sensors*, vol. 19, no. 13, p. 2870, Jun. 2019.
- [13] G. Kutyniok, H. Boche, R. Calderbank, and J. Vybird, *Compressed Sensing and its Applications: MATHEON Workshop 2013*, 07 2015.
- [14] G. Kutyniok, “Theory and applications of compressed sensing,” *GAMM-Mitteilungen*, vol. 36, no. 1, pp. 79–101, Aug. 2013.
- [15] R. G. Baraniuk, “More Is Less: Signal Processing and the Data Deluge,” *Science*, vol. 331, no. 6018, pp. 717–719, 2011.
- [16] E. J. Candes and T. Tao, “Near-Optimal Signal Recovery From Random Projections: Universal Encoding Strategies?” *IEEE Transactions on Information Theory*, vol. 52, no. 12, pp. 5406–5425, 2006.
- [17] L. Welch, “Lower bounds on the maximum cross correlation of signals,” vol. 20, no. 3, pp. 397–399, 1974.
- [18] R. Baraniuk, “Compressive Sensing,” *IEEE Signal Processing Magazine*, vol. 24, no. 4, pp. 118–121, 2007.
- [19] D. Achlioptas, “Database-friendly random projections,” in *Proceedings of the twentieth ACM symposium on Principles of database systems*. Santa Barbara, California, US: ACM Press, 2001, pp. 274–281.
- [20] B. Richard, D. Mark, D. Ronald, and W. Michael, “A Simple Proof of the Restricted Isometry Property for Random Matrices,” *Constructive Approximation*, vol. 28, no. 3, pp. 253–263, 2008.
- [21] J. G. P. E. B. O. H. F. Astaiza Hoyos, Evelio, “Compressive sensing: A methodological approach to an efficient signal processing,” *DYNA*, vol. 82, no. 192, pp. 203–210, 2015.
- [22] L. Rudin, S. Osher, and E. Fatemi, “Nonlinear total variation based noise removal algorithms,” *Physica D: Nonlinear Phenomena*, vol. 60, pp. 259–268, 11 1992.
- [23] B. S. P. and V. Lieven, *Convex optimization*. Cambridge, UK; New York: Cambridge University Press, 2004.
- [24] J. Romberg, “Imaging via Compressive Sampling,” *IEEE Signal Processing Magazine*, vol. 25, no. 2, pp. 14–20, 2008.
- [25] C. Emmanuel and R. Justin, “ ℓ_1 -magic: Recovery of sparse signals via convex programming,” pp. 1–19, 2005.